Dynamical density-matrix renormalization group for the Mott–Hubbard insulator in high dimensions

2004 J. Phys.: Condens. Matter 16 7063

(http://iopscience.iop.org/0953-8984/16/39/038)

INSTITUTE OF PHYSICS PUBLISHING JOURNAL OF PHYSICS: CONDENSED MATTER

J. Phys.: Condens. Matter **16** (2004) 7063–7081 PII: S0953-8984(04)82814-5

Dynamical density-matrix renormalization group for the Mott–Hubbard insulator in high dimensions

Satoshi Nishimoto[1], **Florian Gebhard**[1] **and Eric Jeckelmann**[2]

[1] Fachbereich Physik, Philipps-Universität Marburg, D-35032 Marburg, Germany
[2] Institut für Physik, KOMET 337, Johannes Gutenberg-Universität Mainz, 55099 Mainz, Germany

E-mail: Florian.Gebhard@Physik.Uni-Marburg.DE

Received 29 June 2004
Published 17 September 2004
Online at stacks.iop.org/JPhysCM/16/7063
doi:10.1088/0953-8984/16/39/038

Abstract

We study the Hubbard model at half band-filling on a Bethe lattice with infinite coordination number in the paramagnetic insulating phase at zero temperature. We use the dynamical mean-field theory (DMFT) mapping to a single-impurity Anderson model with a bath whose properties have to be determined self-consistently. For a controlled and systematic implementation of the self-consistency scheme we use the fixed-energy approach to the DMFT (FE-DMFT). In FE-DMFT, the onset and the width of the Hubbard bands are adjusted self-consistently but the energies of the bath levels are kept fixed relatively to both band edges during the calculation of self-consistent hybridization strengths between impurity and bath sites. Using the dynamical density-matrix renormalization group method (DDMRG) we calculate the density of states with a resolution ranging from 3% of the bare bandwidth $W = 4t$ at high energies to 0.5% in the vicinity of the gap. The DDMRG resolution and accuracy for the density of states and the gap is superior to those obtained with other numerical methods in previous DMFT investigations. We find that the Mott gap closes at a critical coupling $U_c/t = 4.45 \pm 0.05$. At $U = 4.5t$, we observe prominent shoulders near the onset of the Hubbard bands. They are the remainders of the quasi-particle resonance in the metallic phase which appears to split when the gap opens at U_c.

1. Introduction

In the limit of high dimensions [1], models for correlated lattice electrons can be mapped onto effective single-impurity problems [2, 3]. In some cases, the exact solution for a many-particle Hamiltonian has been found, e.g., for the Falicov–Kimball model [2, 4], and for other problems a few exact results have been obtained; for reviews, see [5, 6]. Despite its increasing

popularity [5, 7, 8], it must be kept in mind that the dynamical mean-field theory (DMFT) still poses a difficult many-body problem: the effective single-impurity model must be solved self-consistently for the one-particle Green function at all frequencies. Consequently, reliable numerical or analytical 'impurity solvers' must be developed and the self-consistency scheme must be implemented in a controlled way.

The Hubbard model at half band-filling provides an ideal test case for the DMFT. It describes s-electrons with a purely local interaction of strength U and electron transfer matrix elements $-t/\sqrt{Z}$ between $Z \to \infty$ neighbouring sites on a lattice. On the one hand, the model contains an interesting quantum phase transition between the paramagnetic metal and the paramagnetic (Mott–Hubbard) insulator [9] at a finite coupling. On the other hand, for a Bethe lattice with a semi-elliptic bare density of states of width $W = 4t$, perturbation theory to fourth order in U/W [10] and to second order in W/U [11] have been carried out at zero temperature, against which approximate analytical and numerical techniques can be tested. In this way, merits and limitations of analytical methods (Hubbard-III approximation [12], iterated perturbation theory [13], local moment approach [14]) and numerical techniques (exact diagonalization schemes (ED) [15, 16], numerical renormalization group (NRG) [17]) have been revealed, together with the difficulties in implementing the self-consistency scheme in numerical approaches.

The latter problem results from the fact that numerical approaches work with a finite number of sites to represent the continuous bath coupled to the impurity site. Thus the energy resolution is necessarily limited by finite-size effects. Moreover, it is not clear *a priori* how one can define a self-consistency condition for the discretized impurity problem such that the self-consistent solution is approached in a smooth and controlled way in the limit of an infinite number of bath sites. (In other approaches to the impurity problem, such as quantum Monte Carlo (QMC) simulations, the bath is not discretized but the imaginary time has to be discretized, which leads to similar problems.) In a previous work [10, 11], this problem has been solved by the 'fixed-energy' approach to the FE-DMFT: (i) a frequency interval I is split into subintervals I_ℓ of equal length, whose mid-points ϵ_ℓ give the energies of the bath sites, and the density of states is put to zero outside this interval I; (ii) the hybridization strengths between impurity and bath sites is determined self-consistently for these fixed energies ϵ_ℓ. Within the fixed-energy approach to DMFT, the resolution of the frequency interval I improves systematically with system size n_s, and an extrapolation $n_s \to \infty$ becomes meaningful. As has been shown in [10, 11], the FE-DMFT combined with ED [FE-DMFT(ED)] with $n_s \leqslant 15$ provides a reasonable description of the metallic phase for $U \leqslant 0.4W$ and of the Mott–Hubbard insulator for $U/W \geqslant 1.2$.

With ED, finite-size effects are prominent in the interesting region of the metal–insulator transition, i.e., for $U \approx W$. Consequently, numerical approaches are required which overcome the limitation of the ED technique. The dynamical density-matrix renormalization group method (DDMRG) [18] treats large systems (here with up to $n_s = 161$ sites) very accurately. It is an extension of the standard density-matrix renormalization group (DMRG) [19, 20] to the calculation of dynamical correlation functions. For the computation of a continuous spectrum, DDMRG is more efficient than previous generalizations of the DMRG to dynamical quantities such as the Lanczos-DMRG [21], or the correction-vector DMRG [22]. The DDMRG has been applied successfully to the single-impurity Anderson model [23] and to DMFT calculations for the metallic phase of the Hubbard model [10].

In this work, we present results for the Mott–Hubbard insulator on a Bethe lattice with $Z \to \infty$ neighbours obtained with FE-DMFT combined with DDMRG (FE-DMFT(DDMRG)). In section 2 we specify the Hubbard model, the effective single-impurity Hamiltonian, the corresponding one-particle Green functions, and the self-consistency condition. We also recall

the results from perturbation theory in $1/U$. In section 3 we summarize important aspects of the fixed-energy approach to the DMFT, and the DDMRG impurity solver. Details can be found in [10, 11, 23]. In section 4 we display the density of states, the gap for single-particle excitations, the ground-state energy and the average double occupancy as a function of the interaction strength U in the Mott insulating phase found for $U > U_c = 4.45(\pm 0.05)t$. A short summary and conclusions complete our presentation. A sum rule for the ground-state energy of the single-impurity Anderson model at self-consistency is derived in an appendix.

2. Definitions

2.1. Hamiltonian

We investigate spin-1/2 electrons on a lattice whose motion is described by

$$\hat{T} = \sum_{\vec{i},\vec{j};\sigma} t_{\vec{i},\vec{j}} \hat{c}^{+}_{\vec{i},\sigma} \hat{c}_{\vec{j},\sigma}, \tag{1}$$

where $\hat{c}^{+}_{\vec{i},\sigma}$, $\hat{c}_{\vec{i},\sigma}$ are creation and annihilation operators for electrons with spin $\sigma = \uparrow, \downarrow$ on site $\vec{i}$. The matrix elements $t_{\vec{i},\vec{j}}$ are the electron transfer amplitudes between sites $\vec{i}$ and $\vec{j}$, and $t_{\vec{i},\vec{i}} = 0$. Since we are interested in the Mott insulating phase, we consider exclusively a half-filled band where the number of electrons N equals the number of lattice sites L.

For lattices with translational symmetry, $t_{\vec{i},\vec{j}} = t(\vec{i} - \vec{j})$, the operator for the kinetic energy is diagonal in momentum space,

$$\hat{T} = \sum_{\vec{k},\sigma} \epsilon(\vec{k}) \hat{c}^{+}_{\vec{k},\sigma} \hat{c}_{\vec{k},\sigma}, \tag{2}$$

where

$$\epsilon(\vec{k}) = \frac{1}{L} \sum_{\vec{i},\vec{j}} t(\vec{i} - \vec{j}) \mathrm{e}^{-\mathrm{i}(\vec{i}-\vec{j})\vec{k}}. \tag{3}$$

The density of states for non-interacting electrons is then given by

$$\rho(\epsilon) = \frac{1}{L} \sum_{\vec{k}} \delta(\epsilon - \epsilon(\vec{k})). \tag{4}$$

In the limit of infinite lattice dimensions and for translationally invariant systems without nesting, the Hubbard model is characterized by $\rho(\epsilon)$ alone, i.e. higher-order correlation functions in momentum space factorize [24]. For our explicit calculations we shall later use the semi-circular density of states

$$\rho_0(\omega) = \frac{2}{\pi W} \sqrt{4 - \left(\frac{4\omega}{W}\right)^2} \qquad \left(|\omega| \leqslant \frac{W}{2}\right), \tag{5}$$

$$1 = \int_{-W/2}^{W/2} \mathrm{d}\omega \, \rho_0(\omega), \tag{6}$$

where $W = 4t$ is the bandwidth. In the following, we take $t \equiv 1$ as our unit of energy. This density of states is realized for non-interacting tight-binding electrons on a Bethe lattice of connectivity $Z \to \infty$ [25]. Specifically, each site is connected to Z neighbours without generating closed loops, and the electron transfer is restricted to nearest neighbours,

$t_{\vec{i},\vec{j}} = -t/\sqrt{Z}$ when $\vec{i}$ and $\vec{j}$ are nearest neighbours and zero otherwise. The limit $Z \to \infty$ is implicitly understood henceforth.

The electrons are taken to interact only locally, and the Hubbard interaction reads

$$\hat{D} = \sum_{\vec{i}} \left(\hat{n}_{\vec{i},\uparrow} - \frac{1}{2} \right) \left(\hat{n}_{\vec{i},\downarrow} - \frac{1}{2} \right), \tag{7}$$

where $\hat{n}_{\vec{i},\sigma} = \hat{c}^{+}_{\vec{i},\sigma} \hat{c}_{\vec{i},\sigma}$ is the local density operator at site $\vec{i}$ for spin σ. This leads us to the Hubbard model [26],

$$\hat{H} = \hat{T} + U\hat{D}. \tag{8}$$

The Hamiltonian explicitly exhibits particle–hole symmetry, i.e., $\hat{H}$ is invariant under the particle–hole transformation

$$\hat{c}^{+}_{\vec{i},\sigma} \mapsto (-1)^{|\vec{i}|} \hat{c}_{\vec{i},\sigma}, \qquad \hat{c}_{\vec{i},\sigma} \mapsto (-1)^{|\vec{i}|} \hat{c}^{+}_{\vec{i},\sigma}, \tag{9}$$

where $|\vec{i}|$ counts the number of nearest-neighbour steps from the origin of the Bethe lattice to site $\vec{i}$. The chemical potential $\mu = 0$ then guarantees a half-filled band for all temperatures [6].

2.2. Green functions

The time-dependent local single-particle Green's function at zero temperature is given by [27]

$$G(t) = -\mathrm{i} \frac{1}{L} \sum_{\vec{i},\sigma} \langle \hat{\mathcal{T}} [\hat{c}_{\vec{i},\sigma}(t) \hat{c}^{+}_{\vec{i},\sigma}] \rangle. \tag{10}$$

Here $\hat{\mathcal{T}}$ is the time-ordering operator and $\langle \cdots \rangle$ implies the average over the degenerate ground states with energy E_0, and (taking $\hbar \equiv 1$ henceforth)

$$\hat{c}_{\vec{i},\sigma}(t) = \exp(\mathrm{i}\hat{H}t) \hat{c}_{\vec{i},\sigma} \exp(-\mathrm{i}\hat{H}t) \tag{11}$$

is the annihilation operator in the Heisenberg picture.

In the insulating phase, we can readily identify the contributions from the lower (LHB) and upper (UHB) Hubbard bands to the Fourier transform of the local Green function ($\eta = 0^{+}$),

$$\begin{aligned} G(\omega) &= \int_{-\infty}^{\infty} \mathrm{d}t \, \mathrm{e}^{\mathrm{i}\omega t} G(t) = G_{\mathrm{LHB}}(\omega) + G_{\mathrm{UHB}}(\omega), \\ G_{\mathrm{LHB}}(\omega) &= \frac{1}{L} \sum_{\vec{i},\sigma} \langle \hat{c}^{+}_{\vec{i},\sigma} [\omega + (\hat{H} - E_0) - \mathrm{i}\eta]^{-1} \hat{c}_{\vec{i},\sigma} \rangle, \\ G_{\mathrm{UHB}}(\omega) &= -G_{\mathrm{LHB}}(-\omega). \end{aligned} \tag{12}$$

The last equality follows from the particle–hole symmetry (9). Therefore, it is sufficient to evaluate the local Green function for the lower Hubbard band which describes the dynamics of a hole inserted into the system.

The density of states for the lower Hubbard band can be obtained from the imaginary part of the Green function (12) for real arguments via [27]

$$D_{\mathrm{LHB}}(\omega) = \frac{1}{\pi} \Im G_{\mathrm{LHB}}(\omega) = \frac{1}{L} \sum_{\vec{i},\sigma} \langle \hat{c}^{+}_{\vec{i},\sigma} \delta(\omega + \hat{H} - E_0) \hat{c}_{\vec{i},\sigma} \rangle, \tag{13}$$

with $\omega \leqslant -\Delta(U)/2 < 0$, where $\Delta(U)$ is the single-particle gap. Particle–hole symmetry results in a symmetric density of states around $\omega = 0$ at half band-filling

$$D(\omega) = D_{\mathrm{LHB}}(\omega) + D_{\mathrm{UHB}}(\omega) \tag{14}$$

with $D_{\mathrm{UHB}}(\omega) = D_{\mathrm{LHB}}(-\omega)$.

We define the (shifted) moments $M_n(U)$ of the density of states in the lower Hubbard band via

$$M_n(U) = \int_{-\infty}^{-\Delta(U)/2} \mathrm{d}\omega \left(\omega + \frac{U}{2}\right)^n D_{\mathrm{LHB}}(\omega). \tag{15}$$

In particular, from (13), we find that [27]

$$M_0(U) = 1, \tag{16}$$

$$M_1(U) = \frac{1}{L}\left(E_0(U) + U\frac{\partial E_0(U)}{\partial U}\right) + \frac{U}{2} \tag{17}$$

are two useful sum rules which we shall employ later. We also note that the average double occupancy is related to a derivative of the ground-state energy by

$$d(U) = \frac{1}{4} + \frac{1}{L}\langle \hat{D} \rangle = \frac{1}{4} + \frac{1}{L}\frac{\partial E_0(U)}{\partial U}. \tag{18}$$

2.3. Results from strong-coupling perturbation theory

We shall test our numerical results against those from strong-coupling perturbation theory [11]. To second order in $1/U$, the density of states of the lower Hubbard band reads

$$\begin{aligned} D_{\mathrm{LHB}}(\omega) &= \int_{-2}^{2} \mathrm{d}\epsilon\, \rho_0(\epsilon) s(\epsilon, U) \delta\left(\omega + \frac{U}{2} + g(\epsilon, U)\right) + \mathcal{O}(U^{-3}), \\ s(\epsilon, U) &= 1 - \frac{\epsilon}{U} + \frac{9(\epsilon^2 - 1)}{4U^2}, \qquad g(\epsilon, U) = \epsilon - \frac{\epsilon^2 - 3}{2U} + \frac{3\epsilon(2\epsilon^2 - 7)}{8U^2}. \end{aligned} \tag{19}$$

The zeros of $D_{\mathrm{LHB}}(\omega)$ provide the single-particle gap and the width of the Hubbard bands $W^*(U)$,

$$\Delta(U) = U - 4 - \frac{1}{U} - \frac{3}{2U^2} + \mathcal{O}(U^{-3}), \tag{20}$$

$$W^*(U) = 4 + \frac{3}{2U^2} + \mathcal{O}(U^{-3}) \tag{21}$$

up to second order in $1/U$. The Hubbard bands display a square-root onset,

$$D_{\mathrm{UHB}}(\omega) \sim \left(\omega - \frac{\Delta(U)}{2}\right)^{1/2}, \qquad \omega \to \frac{\Delta(U)}{2}. \tag{22}$$

Note that there is no weight outside the Hubbard bands up to and including order $1/U^3$ but there are contributions to order $1/U^4$ and higher. Our numerical results show that the weight outside the (primary) Hubbard bands at $|\omega| \geqslant \Delta(U)/2 + W^*(U)$ is at most 1% of the total density of state for all interaction strengths in the insulating phase.

Recently, Kalinowski and co-workers [28, 29] calculated the ground-state energy to 11th order in the inverse coupling strength. Here we restate their results:

$$\frac{E_0(U)}{L} = -\frac{U}{4} - \frac{1}{2U} - \frac{1}{2U^3} - \frac{19}{8U^5} - \frac{593}{32U^7} - \frac{23877}{128U^9} - \frac{4496245}{2048U^{11}} - \mathcal{O}(U^{-13}), \tag{23}$$

$$d(U) = \frac{1}{2U^2} + \frac{3}{2U^4} + \frac{95}{8U^6} + \frac{4151}{32U^8} + \frac{214893}{128U^{10}} + \frac{49458695}{2048U^{12}} + \mathcal{O}(U^{-14}). \tag{24}$$

Unfortunately, the computational effort increases exponentially as a function of the order, and it will be difficult to obtain much higher orders of the expansion.

3. FE-DMFT(DDMRG)

In this section, we first discuss the single-impurity model onto which the Hubbard model can be mapped in the limit of infinite dimensions. Next, we recall the fixed-energy algorithm for the DMFT. Lastly, we discuss the DMRG for the numerical solution of the single-impurity Anderson model.

3.1. DMFT

In the limit of infinite dimensions [1], and under the conditions of translational invariance and convergence of perturbation theory in strong and weak coupling, the Hubbard model can be mapped onto single-impurity models [2, 3, 5], which need to be solved self-consistently. In general, these impurity models cannot be solved analytically.

For an approximate numerical treatment various different implementations are conceivable. One realization is the single-impurity Anderson model in 'star geometry',

$$\begin{aligned}\hat{H}_{\mathrm{SIAM}} = &\sum_{\ell=1;\sigma}^{n_s-1} \epsilon_\ell \hat{\psi}^+_{\sigma;\ell}\hat{\psi}_{\sigma;\ell} + U\left(\hat{d}^+_\uparrow\hat{d}_\uparrow - \frac{1}{2}\right)\left(\hat{d}^+_\downarrow\hat{d}_\downarrow - \frac{1}{2}\right) \\ &+ \sum_\sigma \sum_{\ell=1}^{n_s-1} V_\ell(\hat{\psi}^+_{\sigma;\ell}\hat{d}_\sigma + \hat{d}^+_\sigma\hat{\psi}_{\sigma;\ell}),\end{aligned} \tag{25}$$

where V_ℓ are real, positive hybridization matrix elements. The model describes the hybridization of an impurity site with Hubbard interaction to n_s-1 bath sites without interaction at energies ϵ_ℓ. Here $\hat{d}^+_\sigma, \hat{d}_\sigma, \hat{\psi}^+_{\sigma;\ell}, \hat{\psi}_{\sigma;\ell}$ are creation and annihilation operators for electrons with spin $\sigma = \uparrow, \downarrow$ on the impurity and the bath site ℓ, respectively. In order to ensure particle–hole symmetry, we have to set $\epsilon_\ell = -\epsilon_{n_s-\ell}$ and $V_\ell = V_{n_s-\ell}$ for $\ell = (n_s+1)/2, \ldots, n_s - 1$. Moreover, since we are interested in the Mott–Hubbard insulator, we only use odd n_s so that there is no bath state at $\epsilon = 0$.

For a given set of parameters $\{\epsilon_\ell, V_\ell\}$ the model (25) defines a many-body problem for which the single-particle Green function

$$G^{(n_s)}_{dd;\sigma}(t) = -\mathrm{i}\langle\hat{\mathcal{T}}[\hat{d}_\sigma(t)\hat{d}^+_\sigma]\rangle_{\mathrm{SIAM}} \tag{26}$$

must be calculated numerically. Here, $\langle\ldots\rangle_{\mathrm{SIAM}}$ implies the ground-state expectation value within the single-impurity model.

Ultimately, we are interested in the limit $n_s \to \infty$ where

$$H^{(n_s)}(\omega) = \sum_{\ell=1}^{n_s-1} \frac{V_\ell^2}{\omega - \epsilon_\ell + \mathrm{i}0^+\mathrm{sgn}(\omega)} \tag{27}$$

becomes the hybridization function of the *continuous* problem,

$$H(\omega) = \lim_{n_s \to \infty} H^{(n_s)}(\omega) \tag{28}$$

and the Green function is

$$G_{dd}(\omega) = \lim_{n_s \to \infty} [G^{(n_s)}_{dd;\uparrow}(\omega) + G^{(n_s)}_{dd;\downarrow}(\omega)]. \tag{29}$$

(For finite n_s the Green functions $G^{(n_s)}_{dd;\sigma}(\omega)$ are different for $\sigma = \uparrow, \downarrow$ because the system contains an odd number n_s of electrons.) As shown in [5], the hybridization function and the Green function must obey a self-consistency relation

$$H(\omega) = \frac{G_{dd}(\omega)}{2} \tag{30}$$

to describe the Hubbard model on the Bethe lattice with connectivity $Z \to \infty$. At self-consistency, the Green function of the impurity problem gives the Green function of the Hubbard model,

$$G_{dd}(\omega) = G(\omega). \tag{31}$$

For a finite-size representation of the bath, $n_s < \infty$, it is generally *not* possible to find a self-consistent solution to the finite-system version of (30),

$$H^{(n_s)}(\omega) = \tfrac{1}{2}[G^{(n_s)}_{dd;\uparrow}(\omega) + G^{(n_s)}_{dd;\downarrow}(\omega)]. \tag{32}$$

Instead, we have to choose bath energies ϵ_ℓ and hybridizations V_ℓ for finite n_s in such a way that the single-particle Green function and the hybridization function fulfil (30) for $n_s \to \infty$. Therefore, numerical methods will differ in the way an approximate self-consistency condition is defined. This is a source of ambiguity because there can be more than one self-consistent set of parameters $\{\epsilon_\ell, V_\ell\}$ for a fixed n_s. Moreover, it cannot be guaranteed that different schemes will ultimately coincide for $n_s \to \infty$.

3.2. FE-DMFT

In [11] a new algorithm for solving the self-consistency problem has been introduced. The accuracy and stability of this 'fixed-energy DMFT' approach has been demonstrated using an ED technique as 'impurity solver', i.e. to compute the single-impurity Green function $G^{(n_s)}_{dd,\sigma}(\omega)$. In this work, we describe how to use the FE-DMFT together with the DDMRG as impurity solver.

For the Mott–Hubbard insulator, we make the assumption that all the spectral weight is concentrated in the upper and lower Hubbard bands, i.e. in the finite frequency interval

$$I = \left\{ \omega \,\middle|\, \frac{\Delta(U)}{2} \leqslant |\omega| \leqslant \frac{\Delta(U)}{2} + W^*(U) \right\}. \tag{33}$$

The onset of the upper Hubbard band, $\Delta(U)/2$, and the width of the Hubbard bands, $W^*(U)$, are determined self-consistently; see below. We start with some input guess $\Delta(U)$ and $W^*(U)$, which we may take from second-order perturbation theory (20), from the FE-DMFT with ED [11], or from previous runs for slightly different values of U or n_s. We discretize the Hubbard bands equidistantly, i.e. we fix the energies ϵ_ℓ by

$$\epsilon_\ell = -\epsilon_{n_s-\ell} = \frac{\Delta(U)}{2} + \left(\ell - \frac{1}{2}\right)\delta(U), \qquad 1 \leqslant \ell \leqslant (n_s - 1)/2, \tag{34}$$

where

$$\delta(U) = \frac{2W^*(U)}{n_s - 1} \tag{35}$$

is the distance between two consecutive energies ϵ_ℓ in the same Hubbard band. Then we divide the interval I into $n_s - 1$ intervals I_ℓ of width $\delta(U)$ centred around each energy ϵ_ℓ. By fixing the energies at the centres of equidistant intervals we can be sure that our resolution of the Hubbard bands becomes increasingly better as n_s increases. For a typical $n_s = 65$ and $W^*(U) \approx 4t$ we have $\delta(U) \approx 0.125$.

When we integrate the imaginary part of the Green function over the interval I_ℓ we obtain weights w_ℓ,

$$w_\ell = \int_{I_\ell} \mathrm{d}\omega \frac{|\Im G_{dd}(\omega)|}{2}. \tag{36}$$

At self-consistency (30) and for $n_s \to \infty$, these weights obey

$$V_\ell^2 = w_\ell. \tag{37}$$

We can use this relation to calculate new parameters V_ℓ from a Green function $G_{dd}(\omega)$. As initial values for $G_{dd}(\omega)$ we may again use the result of second-order perturbation theory (19) in (36), the results of the FE-DMFT(ED) [11], or we start from previous runs for slightly different values of U or n_s. The latter approach is recommendable close to the transition.

At every iteration, the impurity Green function $G_{dd}(\omega)$ must be calculated with the help of an 'impurity solver'. Here, we use the dynamical DMRG to calculate $G^{(n_s)}_{dd,\sigma}(\omega)$ for the Hamiltonian (25) with finite n_s. Then, the deconvolution of the sum of these Green functions for $\sigma = \uparrow, \downarrow$ gives an excellent approximation of the Green function $G_{dd}(\omega)$ in the limit $n_s \to \infty$ at all needed frequencies (see the next subsection).

We now describe the iterative procedure used to determine the onset of the upper Hubbard band $\Delta(U)/2$, its width $W^*(U)$, and the Green functions $G_{dd}(\omega)$ self-consistently. Starting from the initial $\Delta(U)/2$, $W^*(U)$ and $G_{dd}(\omega)$, we compute the energies ϵ_ℓ and hybridization matrix elements V_ℓ of the single-impurity Anderson model (25) using equations (34)–(37). In a first calculation, we consider this model with n_s sites and use the DDMRG method to compute the full Green functions $G^{(n_s)}_{dd,\sigma}(\omega)$ with a resolution $\eta \sim \delta(U) \sim 1/n_s$. As explained above, after deconvolution of these Green functions we obtain a new Green function $G_{dd}(\omega)$, which is used in the next iteration. Simultaneously, we use the DDMRG method with a broadening $\eta \ll \delta(U)$ to compute the energy $\Delta(U, n_s')/2$ of the first pole in $G^{(n_s)}_{dd,\sigma}(\omega)$ (i.e., the lowest state contributing to the density of states) for the single-impurity Anderson model with $n_s' \geqslant n_s$ sites. Typically, we calculate $\Delta(U, n_s')$ for $n_s' = 81, 97, 113, 129, 145, 161$. (These calculations can be carried out for larger system sizes than the calculation of the full Green functions because we only need to determine ground-state properties and a small fraction of the Green function spectrum around $\omega \approx \Delta(U)/2$.) After extrapolating to the thermodynamic limit,

$$\Delta(U) = \lim_{n_s' \to \infty} \Delta(U, n_s'), \tag{38}$$

we obtain a new estimate for the onset of the upper Hubbard band, $\Delta(U)/2$, which is used in the next iteration. At the same time we use the sum rule of the appendix for the ground-state energy $E_0^{\mathrm{SIAM}}(U, n_s')$ of the effective single-impurity Anderson model to calculate a new bandwidth,

$$\frac{\Delta(U) + W^*(U)}{2} = \lim_{n_s' \to \infty} \frac{E_0^{\mathrm{SIAM}}(U, n_s')}{n_s'}. \tag{39}$$

After a new gap $\Delta(U)$, bandwidth $W^*(U)$ and Green function $G_{dd}(\omega)$ have been obtained we can start the next iteration. We repeat this procedure until it converges to a fixed point.

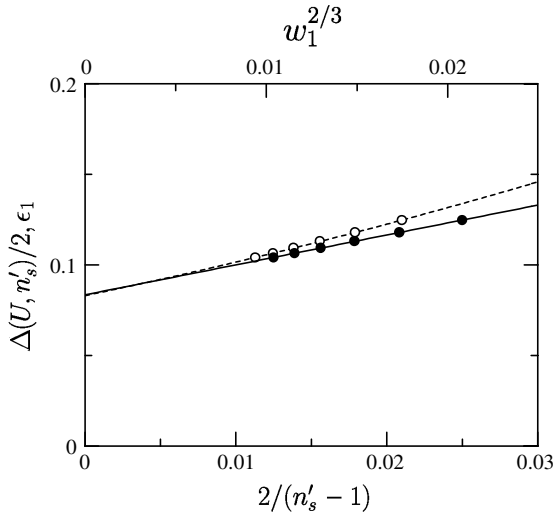

Figure 1. Extrapolation of the lowest lying single-particle excitation energy $\Delta(U,n_s')/2$ as a function of inverse system size (lower axis) for $U = 4.6$ at self-consistency (solid circles). The open circles give the energy ϵ_1 as a function of the weight w_1 (upper axis) for the same system sizes $n_s' = 81, 97, 113, 129, 145, 161$.

Typically, we need less than 10 iterations for the procedure to converge, depending on the choice of the starting parameters. We terminate the iterative procedure when the variation of the gap $\Delta(U)$ and bandwidth $W^*(U)$ are smaller than $10^{-3}t$ from one iteration to the next. At that point the variation of $G_{dd}(\omega)$ is found to be smaller than 10^{-3} for all frequencies ω. This iterative procedure is stable; for small deviations from the self-consistent values, the gap and the width of the Hubbard bands are driven back to the fixed point of the iteration. We have also checked that, for fixed n_s, a unique solution for $G_{dd}(\omega)$ is found for various starting choices. Obviously, our FE-DMFT(DDMRG) approach yields self-consistent results for the gap, bandwidth, and Green function of the Hubbard model. Moreover, it is possible to calculate ground-state properties of the Hubbard model (energy, double occupancy) from ground-state properties of the self-consistent single-impurity Anderson model, as shown in the next section.

In figure 1 we give an example of the extrapolation scheme for $\Delta(U,n_s')$ at the fixed-point of our iterative procedure for $U = 4.6$. As expected, the results for $81 \leqslant n_s' \leqslant 161$ extrapolate linearly in $1/n_s'$. Note that the FE-DMFT with ED [11] was limited to $n_s' = n_s = 15$, and finite-size effects had to be controlled by a combination with the criterion of a square-root onset of the Hubbard bands, which is suggested by perturbation theory (22). The DDMRG treats system sizes up to $n_s' \sim \mathcal{O}(200)$ which makes this 'weight criterion' obsolete. Nevertheless, we can use the 'weight criterion' as a consistency check. As argued in [11], we should find

$$\epsilon_1 - \frac{\Delta(U,n_s')}{2} \propto (w_1)^{2/3}, \tag{40}$$

for a square-root increase in the density of states near the band edges. In figure 1 we show ϵ_1 as a function of $w_1^{2/3}$ for system sizes $81 \leqslant n_s' \leqslant 161$ as open circles. Both extrapolated values for the gap from (38) and (40) agree. The linear behaviour of ϵ_1 as a function of $w_1^{2/3}$ confirms the square-root increase of the density of states near the gap. Note, however, that the region in which the square-root onset is discernible becomes very small close to the transition and thus large system sizes are required.

For $U \leqslant 4.6$, a constant discretization of the Hubbard band with $\delta(U) \approx 0.125$ is not sufficient to resolve fine structures of the density of states near the single-particle gap. In order to obtain a better resolution for $|\omega| \approx \Delta(U)/2$ without excessive increase of the computational effort we use a variable discretization scheme as described in [23]. The resolution around the gap is improved by using a finer discretization $\delta(U)$ of the intervals $\Delta(U)/2 < |\omega| < t$ (i.e., more bath states are used in those intervals). The smaller $\delta(U)$ allows us to use a smaller broadening η in DDMRG calculations for those frequencies. We combine the high-energy spectrum obtained with the usual resolution and the low-energy spectrum obtained with the improved resolution and then deconvolve the result to obtain a new Green function $G_{dd}(\omega)$. This yields $G_{dd}(\omega)$ for $|\omega| < 0.6t$ with a resolution, which is up to an order of magnitude better than that for a constant discretization with $n_s = 65$. For the results presented here we have used $\delta(U) = 0.02$ (corresponding to $n_s = 113$ and $\eta = 0.03$) for $U = 4.5$ and $\delta(U) = 0.031$ ($n_s = 97$ and $\eta = 0.05$) for $U = 4.6$ in the intervals $\Delta(U)/2 < |\omega| < t$.

3.3. DDMRG for the single-impurity Anderson model

The DDMRG for the single-impurity Anderson model is described in detail in [23]. Here, we summarize the essential ingredients. As the DMRG method is most accurate for systems with a quasi one-dimensional structure, we perform calculations of the single-impurity Anderson model (25) in its equivalent linear-chain form [30]

$$\hat{H}_{\mathrm{SIAM}} = U(\hat{d}^{+}_{\uparrow}\hat{d}_{\uparrow} - \tfrac{1}{2})(\hat{d}^{+}_{\downarrow}\hat{d}_{\downarrow} - \tfrac{1}{2}) + V\sum_{\sigma}(\hat{f}^{+}_{\sigma;0}\hat{d}_{\sigma} + \hat{d}^{+}_{\sigma}\hat{f}_{\sigma;0}) + \sum_{\sigma}\sum_{\ell=0}^{n_s-2}\lambda_{\ell}(\hat{f}^{+}_{\sigma;\ell}\hat{f}_{\sigma;\ell+1} + \hat{f}^{+}_{\sigma;\ell+1}\hat{f}_{\sigma;\ell}). \tag{41}$$

The DDMRG provides the local density of states

$$D^{\eta}_{dd,\sigma}(\omega_i) = -\mathrm{sgn}(\omega_i)\frac{\Im G^{(n_s)}_{dd,\sigma}(\omega_i)}{\pi} \tag{42}$$

at selected frequencies ω_i very accurately. The real part of the Green function can also be calculated with DDMRG but to carry out the FE-DMFT calculation we need only the imaginary part. To simulate the continuous spectrum of an infinite chain in a calculation with a finite n_s, a broadening η is introduced which must be scaled as a function of the system size [18]. If η is chosen too small, the density of states displays finite-size peaks as those seen in [31]. If η is chosen too large, relevant information is smeared out. As an empirical fact, $\eta \sim \delta(U) = 2W^{*}(U)/(n_s - 1)$ should be chosen, i.e., the resolution scales as the inverse system size, as found for one-dimensional lattice models [18].

To carry out the iterative procedure described in the previous section, we determine the density of states at selected frequencies ω_i. Typically, we choose them to resolve the effective bandwidth $W^{*}(U)$ equidistantly, $\omega_{i+1} - \omega_i = \delta\omega \approx \eta \sim \delta(U)$. We then 'deconvolve' the DDMRG data by inverting the Lorentz transformation [10]

$$D^{\eta}_{dd}(\omega_i) = \sum_{j}\frac{\delta\omega}{\pi}\frac{\eta}{\eta^2 + (\omega_i - \omega_j)^2}D_{dd}(\omega_j), \tag{43}$$

where $D^{\eta}_{dd}(\omega) = D^{\eta}_{dd,\uparrow}(\omega) + D^{\eta}_{dd,\downarrow}(\omega)$. Through equation (42) this deconvolved density of states $D_{dd}(\omega)$ determines the imaginary part of the Green function $G_{dd}(\omega)$ which is used in the FE-DMFT(DDMRG) scheme. The procedure can be repeated for different choices of the equidistant frequencies ω_j to get more values of $D_{dd,\sigma}(\omega_j)$. In practice, we use two different sets of frequencies, corresponding to a frequency resolution comparable to the bath energy

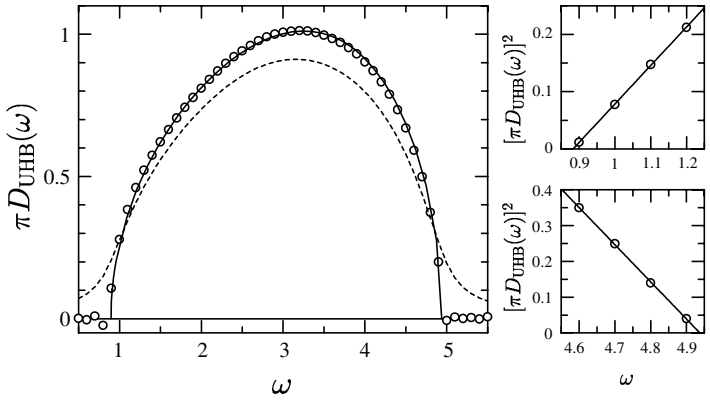

Figure 2. Main figure: density of states of the upper Hubbard band for $U = 6$; - - - -, result of the DDMRG with a broadening $\eta = 0.2$; ○, DDMRG density of states after deconvolution ($\eta = 0$); ——, result from second-order perturbation theory in $1/U$ (19). The side figures show the linear behaviour of the square of the density of states as a function of frequency near the band edges. The lines are linear fits.

resolution $\delta(U)$. In this way, DDMRG provides a set of values $D_{dd,\sigma}(\omega_j)$ for the density of states. The main advantage of this deconvolution is that no extrapolation or finite-size scaling analysis of these values $D_{dd,\sigma}(\omega_j)$ is necessary because they converge very quickly to the $n_s \to \infty$ limit. Naturally, structures with an intrinsic width of less than η cannot be resolved with this procedure even if we use many different sets of frequencies. Therefore, with DDMRG we obtain an accurate discrete representation of the density of states for the continuum model (and thus of the imaginary part of $G_{dd}(\omega)$), except for small regions around its onset and closing points where the derivative of the density of states changes singularly. With the DDMRG method [18], we calculate the one-particle Green function (26) for system sizes up to $n_s \sim \mathcal{O}(200)$. Therefore the FE-DMFT(DDMRG) leads to a much better resolution of the Hubbard bands than our previous FE-DMFT with ED which was limited to $n_s = 15$.

An example of the density of states obtained with the FE-DMFT(DDMRG) approach is shown in figure 2 for $U = 6$. For this interaction strength, the agreement of the deconvolved DDMRG data with the second-order strong-coupling perturbation theory (19) for the Hubbard model is almost perfect. Our deconvolution scheme gives slightly negative values in the vicinity of the band edges. These effects are small and are to be expected for sharp band edges in the density of states at $\omega = \Delta(U)/2$ and $\omega = \Delta(U)/2 + W^*(U)$. We note that our numerical results are in much better agreement with perturbation theory than the results obtained in a recent DMFT(DMRG) study [31] where Lanczos-DMRG and a different self-consistency scheme has been used. Therefore, we think that our results for the gap and the critical interaction strength are also more accurate than those presented in that work [31].

4. Results

In this section we present the results for the Mott insulating phase of the Hubbard model which we have obtained with our FE-DMFT(DDMRG) approach. For ground-state properties comparisons with strong-coupling perturbation theory [11, 28, 29] and DMFT(QMC) results (extrapolated to zero temperature) [28, 32] confirm the accuracy of our method. Moreover,

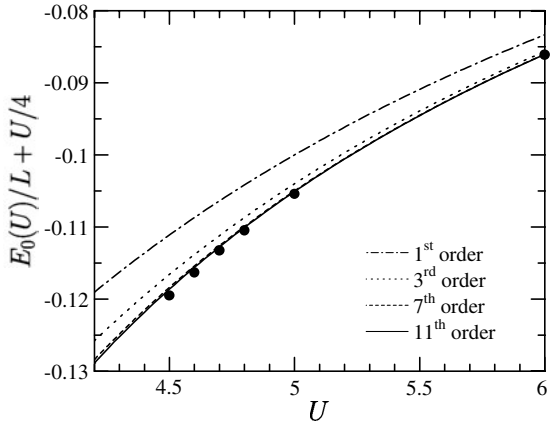

Figure 3. Ground-state energy $E_0/L + U/4$ of the Mott–Hubbard insulator as a function of the interaction strength. FE-DMFT(DDMRG) results for $U = 4.5$, 4.6, 4.7, 4.8, 5, 6 (circles) and perturbation theory (lines) for various orders in $1/U$.

we will present results for the (zero-temperature) single-particle excitations which are much more accurate than those obtained with other DMFT approaches.

4.1. Ground-state properties

The ground-state energy per site of the Hubbard model can be calculated from ground-state expectation values of the self-consistent single-impurity Anderson model (see the appendix)

$$\frac{E_0(U)}{L} + \frac{U}{4} = U\langle \hat{d}^+_\uparrow \hat{d}_\uparrow \hat{d}^+_\downarrow \hat{d}_\downarrow \rangle_{\mathrm{SIAM}} + V\langle \hat{d}^+_\sigma \hat{f}_{0,\sigma} \rangle_{\mathrm{SIAM}}, \tag{44}$$

where the two terms on the right-hand-side are the interaction and kinetic energy per site, respectively, and $V = t = 1$. In figure 3 we show the ground-state energy $E_0(U)/L + U/4$ in the Mott–Hubbard insulator phase for $4.5 \leqslant U \leqslant 6$ in comparison with strong-coupling perturbation theory (23). We see that there is a very good agreement between our numerical data and the analytical results. Our data points lie below the best perturbative energy (11th-order in $1/U$). As expected, deviations from the perturbative results become larger when U becomes smaller, from about 0.8×10^{-4} at $U = 6$ to 8.8×10^{-4} at $U = 4.5$. Our FE-DMFT(DDMRG) energies are also lower than DMFT(QMC) energies [28, 32]. However, the differences are small, of the order of 2×10^{-4} or less, for $U \geqslant 4.8$. As the Mott insulator solution disappears for $U < 4.8$ in the DMFT(QMC) approach, no comparison with our data is possible below that coupling strength.

It is difficult to evaluate the relative accuracy of our method from the ground-state energy alone because that quantity is only defined up to a constant. The average double occupancy of the Hubbard model is given by the average double occupancy of the impurity site in the single impurity Anderson model at self-consistency

$$d(U) = \langle \hat{d}^+_\uparrow \hat{d}_\uparrow \hat{d}^+_\downarrow \hat{d}_\downarrow \rangle_{\mathrm{SIAM}}. \tag{45}$$

At half filling this quantity takes only values between zero and 1/4 and thus provides a good benchmark. In figure 4 we compare our FE-DMFT(DDMRG) results for the average double occupancy with perturbation theory (24) up to 12th order in $1/U$. Again, the agreement is very good but deviations become clearly noticeable for $U < 5$. Quantitatively, the differences between our values for $d(U)$ and the results of the 12th-order perturbation expansion increase

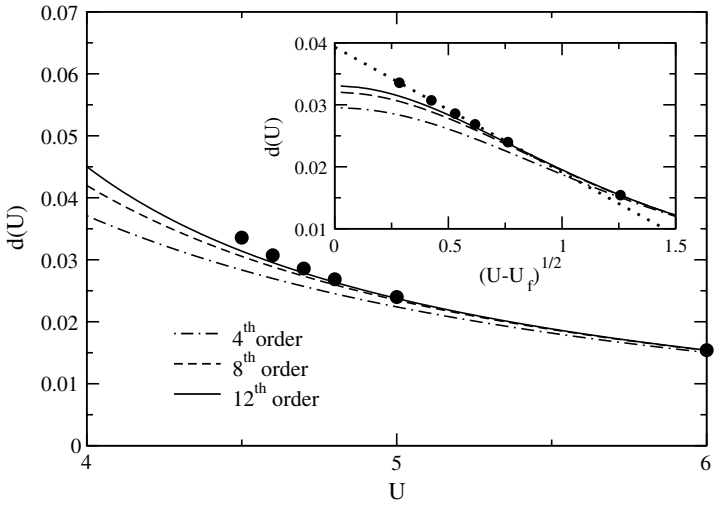

Figure 4. Average double occupancy in the Mott–Hubbard insulator as a function of the interaction strength U. FE-DMFT(DDMRG) results for $U = 4.5$, 4.6, 4.7, 4.8, 5, 6 (circle) and perturbation theory for various orders in $1/U$ (lines). Inset: same results as a function of $(U - U_f)^{1/2}$ with $U_f = 4.419$. The dotted line is a fit to (46).

significantly from 2×10^{-6} (about 0.01%) at $U = 6$ to 2×10^{-3} (about 7%) at $U = 4.5$. This is not surprising because we locate the critical value below which the Mott insulator no longer exists at $U_c \approx 4.45 \pm 0.05$ (see below). The series expansion for the ground-state energy (23) and the average double occupancy (24) converges only for $U > U_c$. Therefore, the results of finite-order perturbation theory rapidly become inaccurate as U approaches U_c. A comparison between FE-DMFT(DDMRG) and DMFT(QMC) [28, 32] data is more conclusive. Both approaches provide results for the average double occupancy which deviate from each other by less than 3×10^{-5}, corresponding to relative errors of the order of 0.1%, down to $U = 4.8$.

With our FE-DMFT(DDMRG) approach the Mott insulator is stable for significantly weaker couplings than predicted by other works [17, 28]. A closer inspection of our data for small $U \leqslant 5$ shows that the double occupancy scales as

$$d(U) = d_f - C\sqrt{U - U_f}. \tag{46}$$

This behaviour is clearly seen in the inset of figure 4. A fit of our data for $U < 5$ gives $U_f = 4.419$, $d_f = 0.03931$ and $C = 0.0202$. Equation (46) suggests that the double occupancy is a singular function of the coupling U at U_f. It is thus reasonable to identify U_f with the critical coupling below which the Mott insulator no longer exists. The value $U_f = 4.419$ is indeed in very good agreement with the coupling $U_c = 4.45 \pm 0.05$ where the Mott gap $\Delta(U)$ closes (see below). As the average double occupancy is related to the ground-state energy by (18), one expects that

$$\frac{E_0(U)}{L} + \frac{U}{4} = e_0 + d_f(U - U_f) - \frac{2C}{3}(U - U_f)^{3/2} \tag{47}$$

for $U \to U_f$. Our data for the ground-state energy for $U < 5$ are reproduced by this formula within 5×10^{-5} if we use $e_0 = 0.12235$ and the parameters d_f, U_f and C determined from the fit of the double occupancy data. Therefore, our FE-DMFT(DDMRG) data for the ground-state energy and the average double occupancy of the Hubbard model with $4.5 \leqslant U < 5$ fulfil the relation (18) very precisely. For an arbitrary single-impurity Anderson model the

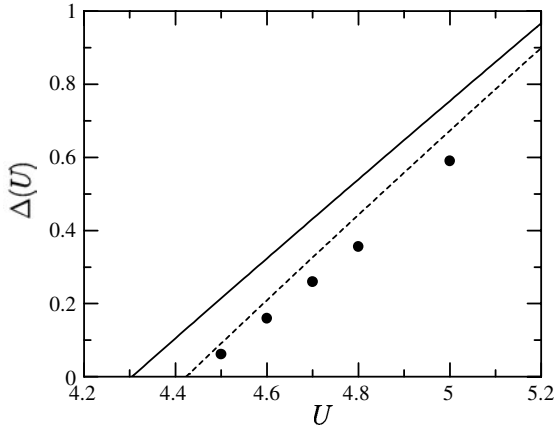

Figure 5. Single-particle gap in the Mott–Hubbard insulator as a function of the interaction strength. FE-DMFT(DDMRG) results (circles), second-order perturbation theory (solid line), and the interpolated result from FE-DMFT(ED) (dashed line).

derivative of the expectation value in the right-hand side of (44) is not given by the average double occupancy (45). The relation (18) between ground-state energy and double occupancy is valid for the Hubbard model and thus only for the expectation values (44) and (45) of the single-impurity Anderson model *at self-consistency*. Therefore, the scalings (46) and (47) of our data confirm that we have found self-consistent DMFT solutions (30) for the Hubbard model with couplings $4.5 \leqslant U < 5$.

Moreover, these results show that our FE-DMFT(DDMRG) approach is accurate enough to allow for an analysis of the critical behaviour and to determine critical exponents for the ground-state energy and the average double occupancy. Note that the behaviour (46) of the average double occupancy implies that the interaction energy $Ud(U)$ scales as $U_f d_f - CU_f\sqrt{U - U_f}$ close to U_f and, consequently, the kinetic energy scales as $K + CU_f\sqrt{U - U_f}$ for small $U - U_f$, where $e_0 = K + U_f d_f$. Recently, evidence for half-integer critical exponents have also been found using an analysis of the strong-coupling perturbation theory extrapolated to infinite order [28]. However, the first singular terms in the expansions of $E_0(U)$ and $d(U)$ were found to have exponents $5/2$ and $3/2$, respectively, compared to $3/2$ and $1/2$ in (47) and (46).

4.2. Single-particle excitations

The single-particle gap $\Delta(U)$ found at the fixed-point of our iterative procedure is shown in figure 5. As expected, $\Delta(U)$ first decreases monotonically with U then vanishes below a finite $U_c > 0$. For $U = 4.5$ the gap $\Delta(U) = 0.062$ is still large enough to be detected with our method but for $U = 4.4$ we find $\Delta(U) = 0$. Thus we estimate that $U_c \approx 4.45$ with an error smaller than 0.05 in full agreement with the singular behaviour of the ground-state energy (47) and double occupancy (46) described above. In figure 5 it is seen that second-order perturbation theory describes the gap behaviour qualitatively but it predicts a vanishing of the gap at a slightly too small $U_c = 4.31$. We also see that our FE-DMFT(DDMRG) results agree with the results from the FE-DMFT(ED) investigation [11]. The small deviations are within the error estimates for FE-DMFT(ED) calculations (see [11]). Concomitantly, the values for the closing of the gap are almost equal, $U_c = 4.43 \pm 0.05$ with the FE-DMFT(ED) method.

Our result for U_c is in conflict with the value $U_c = 4.78$ found using a DMFT(NRG) approach [17] and an analysis of the strong-coupling expansion [28]. In contrast, we find

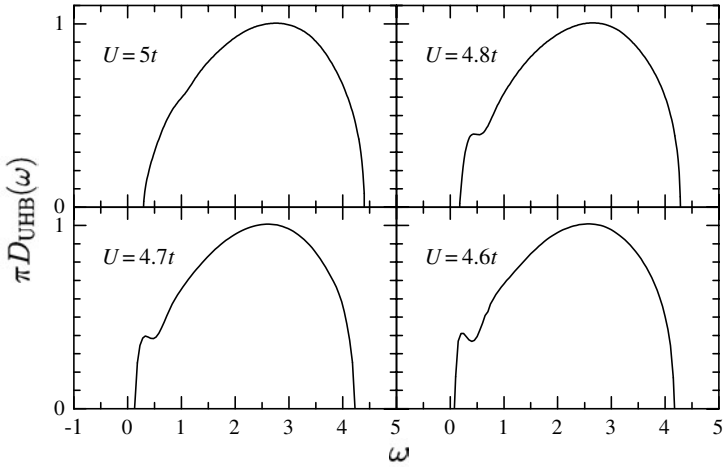

Figure 6. Density of states of the upper Hubbard band for $4.6 \leqslant U \leqslant 5$.

substantial gaps $\Delta(U = 4.8) = 0.356$ and $\Delta(U = 4.7) = 0.260$ just above and below that coupling. These gaps are clearly larger than the discretization of the bath $\delta(U) = 0.125$ that we have used. Therefore, we are confident that $U_c < 4.7$, and that our result $U_c \approx 4.45$ is more reliable than the results of [17, 28].

For large interaction strengths, the derivative of the gap $\Delta(U)$ with respect to U is unity, $\Delta'(U \gg W) = 1$, see (20). For finite U, our results show that $\Delta'(U) > 1$, in agreement with perturbation theory (20). In the vicinity of the transition, $U \approx U_c$, $\Delta'(U)$ again approaches unity and thus $\Delta(U) = U - U_c$.

The width of the Hubbard bands $W^*(U)$ calculated at the fixed-point of the FE-DMFT(DDMRG) procedure is almost constant for all $U > U_c$. At finite coupling it is slightly larger than the value $W^*(U) = W = 4$ predicted by strong-coupling perturbation theory for $U \to \infty$ and reaches a maximum $W^*(U) \approx 4.1$ around $U = 5$.

In order to explain this behaviour, we display the density of states as a function of U in figure 6. For large interaction strengths, $U \geqslant 6$, second-order perturbation theory describes the density of states $D(\omega)$ accurately, as seen in figure 2. The spectrum consists of the two Hubbard bands around $\pm U/2$ with a square-root onset at $\omega = \pm\Delta(U)/2$. For weaker couplings our FE-DMFT(DDMRG) calculations show clearly that a shoulder forms in the density of states near the transition to the metallic phase. In figure 6, we can see that this feature becomes progressively stronger as U approaches U_c. Its appearance is connected with the non-monotonic behaviour of $W^*(U)$ and of $\Delta'(U)$ as a function of U near $U = 5$.

This feature is the remainder of the quasi-particle peak which is present at $\omega = 0$ in the metallic phase. Because the metal is a Fermi liquid, the quasi-particle peak has height $D(\omega = 0) = 2\rho(0) = 2/\pi$ [33]. Figure 7 suggests that the quasi-particle peak splits at the transition to the insulating state at U_c. (A splitting of the density of states at the transition also occurs in the one-dimensional Hubbard model where $U_c = 0^+$, as shown in [34] within a field-theoretical approach.) As the gap opens, the two flanks of the peak quickly lose weight so that they are rather small already at $U = 4.5$.

Clearly, our FE-DMFT(DDMRG) results for the gap and the bandwidth are more accurate and the density of states shown in figures 2–7 have a much better resolution than those calculated with other methods such as the FE-DMFT(ED) [11], DMFT(NRG) [17] or DMFT(DMRG) [31]; DMFT(QMC) calculations [28] have not provided estimates for these quantities. In

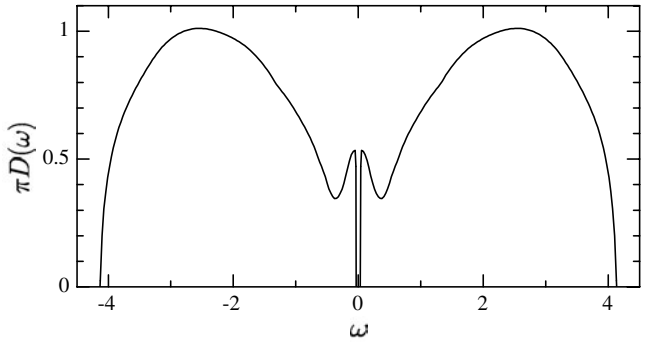

Figure 7. Density of states of the lower and upper Hubbard bands for $U = 4.5$.

particular, our investigation demonstrates the presence of a sharp feature just above the gap in the density of states of the insulator and, thus, provides the first clear evidence for a splitting of the quasi-particle peak at the metal–insulator transition. As an accurate description of the low-energy excitations is necessary close to the critical coupling U_c, it is not surprising that the insulating phase extends to slightly weaker couplings than predicted in previous works [17, 28, 31]. The impurity solvers used in previous DMFT investigations do not have the accuracy of the DDMRG method combined with the FE-DMFT. Therefore, they could not resolve the small gap $\Delta(U) \leqslant 0.260$ for $U \leqslant 4.7$ and did not find a stable insulating phase below that coupling.

5. Summary and conclusions

We have investigated the paramagnetic insulating ground state of the Hubbard model on a Bethe lattice in the limit of infinite coordination number. In this limit, the problem can be treated within the DMFT, i.e. it can be mapped onto a system made of a single impurity with Hubbard interaction and hybridizations to a bath. The system properties have to be determined self-consistently from the required equivalence between the single-particle Green function and the hybridization function. In this work, we have used the fixed-energy approach to the DMFT (FE-DMFT) [11]. The FE-DMFT provides stable solutions of the DMFT self-consistency problem and a systematic convergence of the results with increasing system size.

As 'impurity solver' for the single-particle density of states we have used the dynamical DDMRG [23]. Our results from FE-DMFT(DDMRG) for the ground state agree with perturbation theory in $1/U$, where the latter is applicable, and with QMC simulations, where the DMFT(QMC) approach finds a stable insulating phase. With DDMRG we have used up to 160 sites to represent the self-consistent DMFT bath as compared with $n_s = 15$ with ED. These larger systems provide an enhanced resolution which is necessary to reveal structures in the density of states near the gap. These structures emerge when the Mott gap becomes small, i.e. when the coupling U approaches a critical value U_c below which there is no insulating phase ($\equiv U_{c,1}$ in a scenario with coexisting metallic and insulating phases). Our FE-DMFT(DDMRG) study gives $U_c = 4.45 \pm 0.05$ for the critical interaction strength where the gap closes, in very good agreement with our previous FE-DMFT(ED) study [11], $U_c = 4.43 \pm 0.05$.

In contrast with the results of a recent DMFT(DMRG) work [31], our results are not dominated by finite-size effects. At $U = 6$, for example, the density of states in [31] displays a series of individual peaks instead of the smooth Hubbard bands found in our approach and in perturbation theory. Preliminary results for the metallic Fermi-liquid phase just below U_c

suggest that the narrow quasi-particle resonance simply splits at U_c. Narrow shoulders which can be seen in the insulator density of states for $U = 4.5$ in figure 7 are the remainders of the quasi-particle resonance. The shoulders quickly lose weight as the upper and lower Hubbard bands separate from each other with increasing interaction strength U.

The method presented here can also be applied to the metallic phase, as done in [10] for the weak-coupling limit. It is more difficult to resolve sharp quasi-particle peaks with DDMRG [23] than with, e.g. the NRG. However, as shown in this work, our method offers the unique advantage that we can resolve sharp structures in the vicinity of the Hubbard band onsets. This is very important to describe the Mott insulating phase accurately and to determine the parameter region where it exists. Therefore, we are confident that our FE-DMFT(DDMRG) will provide deeper insight into the Mott–Hubbard metal-to-insulator transition.

Acknowledgments

We thank N Blümer for helpful discussions. This work was supported by the center *Optodynamik* of the Philipps-Universität Marburg.

Appendix. Sum rule

At self-consistency we have from equations (13), (15), (16) and (30)

$$\begin{aligned} M_1(U) - \frac{U}{2} &= \sum_\sigma \int_{\mu^-_{\mathrm{LHB}}}^{\mu^+_{\mathrm{LHB}}} \mathrm{d}\omega\, \omega D_{\mathrm{LHB}}(\omega) \\ &= \sum_\sigma \int_{\mu^-_{\mathrm{LHB}}}^{\mu^+_{\mathrm{LHB}}} \mathrm{d}\omega\, \omega \langle \hat{d}^+_\sigma \delta(\omega + \hat{H}_{\mathrm{SIAM}} - E_0^{\mathrm{SIAM}}) \hat{d}_\sigma \rangle_{\mathrm{SIAM}} \\ &= \sum_\sigma \langle \hat{d}^+_\sigma [\hat{d}_\sigma, \hat{H}_{\mathrm{SIAM}}]_- \rangle_{\mathrm{SIAM}}, \end{aligned} \tag{A.1}$$

where E_0^{SIAM} is the ground-state energy of the single-impurity Anderson model. The fact that the first moments are identical at self-consistency also proves that the average double occupancy of the Hubbard model $d(U)$ is identical to the average double occupancy of the interacting site in the impurity model. Therefore, we do not distinguish between $d(U)$ and $d_{\mathrm{SIAM}}(U)$.

We carry out the commutators in (A.1) using the Hamiltonian (25) and obtain

$$M_1(U) = 2Ud(U) + \sum_{\ell,\sigma} V_\ell \langle \hat{d}^+_\sigma \hat{\psi}_{\ell,\sigma} \rangle_{\mathrm{SIAM}}. \tag{A.2}$$

The ground-state expectation value on the right-hand side of this equation is readily calculated in DMRG. Therefore, combining (17), (18) and (A.2) provides the ground-state energy density of the Hubbard model in terms of the single-impurity results as

$$\frac{E_0(U)}{L} = Ud(U) - \frac{U}{4} + \sum_{\ell,\sigma} V_\ell \langle \hat{d}^+_\sigma \hat{\psi}_{\ell,\sigma} \rangle_{\mathrm{SIAM}}, \tag{A.3}$$

which is equivalent to (44).

The static ground-state expectation value in (A.1) can be obtained from the corresponding Green function. For completeness we define the time-ordered Green functions

$$\begin{aligned} G_{\ell\ell;\sigma}(t) &= -\mathrm{i}\langle \hat{\mathcal{T}}[\hat{\psi}_{\ell,\sigma}(t)\hat{\psi}^+_{\ell,\sigma}] \rangle_{\mathrm{SIAM}}, \qquad G_{\ell d;\sigma}(t) = -\mathrm{i}\langle \hat{\mathcal{T}}[\hat{\psi}_{\ell,\sigma}(t)\hat{d}^+_\sigma] \rangle_{\mathrm{SIAM}}, \\ G_{d\ell;\sigma}(t) &= -\mathrm{i}\langle \hat{\mathcal{T}}[\hat{d}_\sigma(t)\hat{\psi}^+_{\ell,\sigma}] \rangle_{\mathrm{SIAM}}. \end{aligned} \tag{A.4}$$

With the help of the equation of motion it is not difficult to show that their Fourier transforms obey ($\omega \equiv \omega + \mathrm{i}0^+\mathrm{sgn}\,\omega$)

$$G_{\ell\ell;\sigma}(\omega) = \frac{1}{\omega - \epsilon_\ell} + \frac{V_\ell^2}{(\omega - \epsilon_\ell)^2} G_{dd;\sigma}(\omega), \qquad G_{\ell d;\sigma}(\omega) = \frac{V_\ell}{\omega - \epsilon_\ell} G_{dd;\sigma}(\omega) = G_{d\ell;\sigma}(\omega). \tag{A.5}$$

Then, the first moment in (A.2) becomes ($\nu = 0^+$)

$$M_1 = 2Ud(U) + \sum_{\ell,\sigma} V_\ell \int_{-\infty}^{\infty} \frac{\mathrm{d}\omega}{2\pi\mathrm{i}} \mathrm{e}^{\mathrm{i}\omega\nu} \frac{V_\ell}{\omega - \epsilon_\ell} G_{dd;\sigma}(\omega). \tag{A.6}$$

At self-consistency we have (30) which implies

$$\sum_\sigma H(\omega) = \sum_{\ell,\sigma} \frac{V_\ell^2}{\omega - \epsilon_\ell} = G(\omega). \tag{A.7}$$

Therefore, we arrive at the important relation

$$\int_{-\infty}^{\infty} \frac{\mathrm{d}\omega}{2\pi\mathrm{i}} \mathrm{e}^{\mathrm{i}\omega\nu} [G(\omega)]^2 = 2(M_1(U) - 2Ud(U)). \tag{A.8}$$

It relates the ground-state energy of the single-impurity model back to the ground-state energy of the Hubbard model. To show this we start from

$$E_0^{\mathrm{SIAM}}(U) = -\frac{U}{4} + Ud(U) + \sum_{\ell,\sigma} V_\ell \langle \hat{\psi}_{\ell,\sigma}^+ \hat{d}_\sigma + \hat{\psi}_{\ell,\sigma} \hat{d}_\sigma^+ \rangle_{\mathrm{SIAM}} + \sum_{\ell,\sigma} \epsilon_\ell \langle \hat{\psi}_{\ell,\sigma}^+ \hat{\psi}_{\ell,\sigma} \rangle_{\mathrm{SIAM}}. \tag{A.9}$$

With the help of (A.5) and (A.7) we find for the second term in (A.9)

$$\sum_{\ell,\sigma} V_\ell \langle \hat{\psi}_{\ell,\sigma}^+ \hat{d}_\sigma + \hat{\psi}_{\ell,\sigma} \hat{d}_\sigma^+ \rangle_{\mathrm{SIAM}} = 2(M_1(U) - 2Ud(U)). \tag{A.10}$$

For the third term we use

$$\sum_{\ell,\sigma} \frac{V_\ell^2 \epsilon_\ell}{(\omega - \epsilon_\ell)^2} = -H(\omega) - \omega \frac{\partial H(\omega)}{\partial \omega} \tag{A.11}$$

to obtain

$$\begin{aligned} \sum_{\ell,\sigma} \epsilon_\ell \langle \hat{\psi}_{\ell,\sigma}^+ \hat{\psi}_{\ell,\sigma} \rangle_{\mathrm{SIAM}} &= \sum_{\ell,\sigma} \epsilon_\ell \Theta(-\epsilon_\ell) - \frac{1}{2} \int_{-\infty}^{\infty} \frac{\mathrm{d}\omega}{2\pi\mathrm{i}} \mathrm{e}^{\mathrm{i}\omega\nu} G(\omega) \left[G(\omega) + \omega \frac{\partial G(\omega)}{\partial \omega} \right] \\ &= \sum_{\ell,\sigma} \epsilon_\ell \Theta(-\epsilon_\ell) - \frac{1}{2}(M_1(U) - 2Ud(U)). \end{aligned} \tag{A.12}$$

Summing the contributions from (A.10) and (A.12) in (A.9) gives the final result

$$E_0^{\mathrm{SIAM}}(U) = \sum_{\ell,\sigma} \epsilon_\ell \Theta(-\epsilon_\ell) - 2Ud(U) + \frac{3}{2} M_1(U) - \frac{U}{4}, \tag{A.13}$$

where $d(U)$ is the average double occupancy (18), $M_1(U)$ is the first moment (17), and $\Theta(x)$ is the step function. This equation expresses the fact that the impurity provides corrections of order unity to the extensive ground-state energy. Therefore, for our equidistant energy levels ϵ_ℓ we find equation (39).

References

[1] Metzner W and Vollhardt D 1989 *Phys. Rev. Lett.* **62** 324
See also Zaitsev R O and Dushenat M I 1983 *Fiz. Tverd. Tela* **25** 3440
Zaitsev R O and Dushenat M I 1984 *Sov. Phys. Solid State* **25** 1979
[2] Brandt U and Mielsch C 1989 *Z. Phys.* B **75** 365
Brandt U and Mielsch C 1990 *Z. Phys.* B **79** 295
Brandt U and Mielsch C 1991 *Z. Phys.* B **82** 37
[3] Jarrell M 1992 *Phys. Rev. Lett.* **69** 168
[4] Freericks J K and Zlatić V 2003 *Rev. Mod. Phys.* **75** 1333
[5] Georges A, Kotliar G, Krauth W and Rozenberg M J 1996 *Rev. Mod. Phys.* **68** 13
[6] Gebhard F 1997 *The Mott Metal–Insulator Transition* (Berlin: Springer)
[7] Held K, Nekrasov I A, Keller G, Eyert V, Blümer N, McMahan A K, Scalettar R T, Pruschke T, Anisimov V I and Vollhardt D 2002 *Quantum Simulations of Complex Many-Body Systems: From Theory to Algorithms* ed J Grotendorst, D Marx and A Muramatsu *NIC Series* (Juelich: Forschungszentrum Juelich) **10** p 175
[8] Kotliar G and Vollhardt D 2004 *Phys. Today* **57** 73
[9] Mott N F 1990 *Metal–Insulator Transitions* 2nd edn (London: Taylor and Francis)
[10] Gebhard F, Jeckelmann E, Mahlert S, Nishimoto S and Noack R M 2003 *Eur. Phys. J.* B **36** 491
[11] Eastwood M P, Gebhard F, Kalinowski E, Nishimoto S and Noack R M 2003 *Eur. Phys. J.* **35** 155
[12] Hubbard J 1964 *Proc. R. Soc.* **281** 401
[13] Rozenberg M J, Kotliar G and Zhang X Y 1994 *Phys. Rev.* B **49** 10181
[14] Logan D E, Eastwood M P and Tusch M A 1997 *J. Phys.: Condens. Matter* **9** 4211
[15] Caffarel M and Krauth W 1994 *Phys. Rev. Lett.* **72** 1545
Ōno Y, Bulla R, Hewson A C and Potthoff M 2001 *Eur. Phys. J.* B **22** 283
[16] Rozenberg M J, Möller G and Kotliar G 1994 *Mod. Phys. Lett.* B **8** 535
[17] Bulla R 1999 *Phys. Rev. Lett.* **83** 136
Bulla R, Costi T A and Vollhardt D 2001 *Phys. Rev.* B **64** 045103
[18] Jeckelmann E 2002 *Phys. Rev.* B **66** 045114
[19] White S R 1992 *Phys. Rev. Lett.* **69** 2863
White S R 1993 *Phys. Rev.* B **48** 10345
[20] Peschel I, Wang X, Kaulke M and Hallberg K (ed) 1999 *Density-Matrix Renormalization* (Berlin: Springer)
[21] Hallberg K A 1995 *Phys. Rev.* B **52** 9827
[22] Kühner T D and White S R 1999 *Phys. Rev.* B **60** 335
[23] Nishimoto S and Jeckelmann E 2004 *J. Phys.: Condens. Matter* **16** 613
[24] van Dongen P G J, Gebhard F and Vollhardt D 1989 *Z. Phys.* B **76** 199
[25] Economou E 1983 *Green's Functions in Quantum Physics* 2nd edn (Berlin: Springer)
[26] Hubbard J 1963 *Proc. R. Soc.* A **276** 238
Hubbard J 1963 *Proc. R. Soc.* A **277** 237
[27] Fetter A L and Walecka J D 1971 *Quantum Theory of Many-Particle Systems* (New York: McGraw-Hill)
[28] Blümer N and Kalinowski E 2004 *Preprint* cond-mat/0404568
[29] Kalinowski E 2004 private communication
[30] Costi T 1999 *Density-Matrix Renormalization* ed I Peschel, X Wang, M Kaulke and K Hallberg (Berlin: Springer)
[31] García D J, Hallberg K and Rozenberg M J 2004 *Preprint* cond-mat/0403169
[32] Blümer N 2004 private communication
[33] Müller-Hartmann E 1989 *Z. Phys.* B **74** 507
Müller-Hartmann E 1989 *Z. Phys.* B **76** 211
[34] Essler F H L and Tsvelik A M 2002 *Phys. Rev.* B **65** 115117